

Analysis of Vertical Take - off & Landing Aircraft using CFD

S. Rajiv Rao¹

¹Mechanical department
Chaitanya Bharathi Institute of Technology
Hyderabad,India.

Sarla Srinath²

²Mechanical department
Chaitanya Bharathi Institute of Technology
Hyderabad,India.

Vajrala Bhargavi³

³Mechanical department
Chaitanya Bharathi Institute of Technology
Hyderabad,India.

Bharathraj Reddy Dere⁴

⁴Mechanical department
Chaitanya Bharathi Institute of Technology
Hyderabad,India.

ABSTRACT: The concept of a vertical take-off and landing (VTOL) vehicle has been in the literature for almost a century now. This report discusses about the Design and Computational Fluid Dynamics of VTOL aircraft. A vertical take-off and landing (VTOL) aircraft is a type of aircraft that can hover, take off, and land vertically. Our project is on a tilt rotor type aircraft. The V-22 Osprey is a tiltrotor aircraft designed to operate under a wide range of flight conditions. Its outer mold line geometry is aerodynamically complex in part because aerodynamic considerations were not primary influential factors for the major features of the aircraft. As mission requirements change and additional devices are added to the aircraft, questions regarding the aerodynamic impact must be answered. While many of these questions can be adequately answered using lower-fidelity methods, some situations require the use of higher-fidelity analysis. Computational fluid dynamics (CFD) is a tool that has been used frequently to answer aerodynamic questions associated with the V-22. However, the complexity of the aircraft makes this analysis challenging. Using unstructured grids is one way of reducing the lead time required to setup the simulation as unstructured grids lend themselves to modelling complex geometries. This project compares CFD analysis done using a combination of text references and computer tools of the Osprey V-22 tilt rotor in airplane mode over a range of angles of attack, and compares these results to data from a standard journal. The results lend insight into the choice of grid structure and numerical methodology, and reveal that care must be taken when setting up the CFD model as well as identifying any numerical phenomena that could be considered.

CHAPTER 1

INTRODUCTION

The Bell Boeing V-22 Osprey is an American multi-mission, military, tilt rotor aircraft with both a vertical take-off and landing (VTOL), and short take-off and landing (STOL) capability. It is designed to combine the functionality of a conventional helicopter with the long-range, high-speed cruise performance of a turboprop aircraft.

DESIGN

The Osprey is the world's first production tilt rotor aircraft, with one three-bladed prop-rotor, turboprop engine, and transmission nacelle mounted on each wingtip. It is classified as a powered lift aircraft. For take-off and landing, it typically operates as a helicopter with the nacelles vertical and rotors horizontal. Once airborne, the nacelles rotate forward 90° in as little as 12 seconds for horizontal flight, converting the V-22 to a more fuel efficient, higher speed turboprop aircraft. STOL rolling-take-off and landing capability is achieved by having the nacelles tilted forward up to 45°. Other orientations are possible, such as the "80 Jump" take-off which uses nacelles at 80° to quickly achieve high altitude and speed. The fixed wing flight is higher than typical helicopter missions allowing longer range line-of-sight communications for improved command and control.

During the design phase, the overall dimensions of the aircraft were defined by shipboard compatibility requirements (for example to operate, fold and stow on an LHA-class ship; and to carry an F-404 engine internally¹). The wing thickness, sweep, and dihedral were also determined by non-aerodynamic considerations². Extensive wind-tunnel testing in the 1980s helped shape the wing-fuselage juncture, over wing fairing, rear fuselage upsweep, and tail configuration. The current MV-22 Block B configuration has several shape changes including nacelle and spinner; and fuselage sponson. Many avionic kits and antennae are housed in fairings that protrude throughout the fuselage.

Composite materials make up 43% of the V-22's airframe. The prop rotors blades also use composites. For compact storage and transport, partly on Marine launch ships, the V-22's rotors fold in 90 seconds and its wing rotates to align, front-to-back, with the fuselage. Due to the requirement of folding the rotors, their 38 feet diameter is 5 feet less than optimal for vertical take-off, resulting in high disk loading. Most Osprey missions use fixed wing

flight 75% or more of the time, reducing wear and tear on the aircraft and reducing operational costs. This fixed wing flight is higher than typical helicopter missions allowing longer range line-of-sight communications for improved command and control.



Fig 1.1 The Osprey V22

PROPULSION:

The V-22's two Rolls-Royce AE 1107C engines are connected by drive shafts to a common central gearbox so that one engine can power both prop rotors if an engine failure occurs. However, if a prop rotor gearbox fails that prop rotor cannot be feathered, and both engines must be stopped before an emergency landing. The aircraft's autorotation characteristics are poor partly because the rotors have low inertia.

The V-22 has a maximum rotor downwash speed above 80 knots, more than the 64 knots lower limit of a hurricane. The rotor wash usually prevents usage of the starboard door in hover, instead the rear ramp is used for rappelling and hoisting. Boeing has stated the V-22 design loses 10% of its vertical lift over a tilt wing design when operating in helicopter mode because of airflow resistance due to the wings, but that the tilt rotor design has better short take-off and landing performance.

Aerodynamics of V22:

Although every attempt was made to optimize the aerodynamics of the V-22, engineering development involving design to improve shipboard suitability, survivability, reliability and fleet operations have resulted in aerodynamic compromises that caused loss in air-vehicle performance. As a result, design changes were incurred during Engineering Manufacturing Development to regain flight envelope. For instance, external wing fences, fore body strakes and vortex generators were added to increase low-speed and high-speed performance envelope. Computational fluid dynamics (CFD) offers practical and timely analysis to address many aerodynamic designs. Though CFD methods are capable of capturing these aerodynamic interactions, application of these methods pose a challenge and proper care and modelling is required; grids designed for specific flow conditions or grid adaption techniques are sometimes required. The Idea of this project is to conduct a CFD analysis on the osprey V22 Model using a combination of text references and computer tools of the Osprey V-22 tilt rotor in airplane mode over a range of angles of attack, and comparing these results to data from a standard journal.

CHAPTER 2

LITERATURE REVIEW

The V-22 Osprey is a multi-service, multi-mission tilt rotor aircraft capable of operating in many diverse flight conditions. It is designed to take-off and land as a helicopter and fly like a turboprop airplane. This project mainly deals with the Fluid flow analysis over the Osprey V22 and Variation of C_L & C_D with the different angle of attack of the aircraft. It also includes solid modelling of the aircraft.

The modelling of the Osprey V22 is done from the website grabcad.com [7], where in one can find the required model for their need and download and use it or use the reverse engineering process to make replica or make it again. In this current project the reverse engineering technique is used and the model is once again made so that there won't be any fault in the geometry. The dimensions can be used from the same method mentioned above.

The Books Aerodynamics, Aeronautics and Flight Mechanics [4] by Barnes W. McCormick helped us to understand the basic principles of flight dynamics, statics, lift & drag theory of aeroplanes and Basic aerodynamics off VTOL. The Book Aircraft Design[3] – a conceptual approach By Raymer helped us in understanding the basic about conceptual design, configuration layout, propulsion, structure, payload and weights airfoil geometry.

The Book Computational Fluid Dynamics[2] by John D. Anderson provides us basics of CFD, various simulation and experimental techniques used, turbulence models, various mesh adaptation techniques and theoretical approach towards our project.

As far as the simulation is concerned, starting from the work conducted by Robert Narducci & Jennifer Abras in their paper **Analysis of CFD Modelling Techniques over the MV-22 Tilt rotor** [1], compares independent CFD analyses of the MV-22 in airplane mode. Two CFD codes, a structured code, OVERFLOW 2.1, and an unstructured code, FUN3D 10.8 are utilized to generate solutions over a range of angles of attack for conditions corresponding to 200-knot flight along with wind tunnel test on the Osprey V22 model. This initial validation study primarily compares the total lift, drag, and pitching moment on the aircraft as a function of angle of attack.

The V-22 tilt rotor aircraft experiences a download in hover mode decreasing the aircraft's efficiency in this mode. This download is caused by the wing surface obstructing the rotor downwash. The paper "A CFD Analysis of the Download Reduction for the V-22 Osprey Wing" [5] explores the reduction of this download via circulation control. The analysis was completed using computational fluid dynamics.

The Help Tutorial Guide of ANSYS Fluent 14[6], where in the detailed use of the models, boundary conditions, etc., is explained. Some of the articles in the magazine of Cd-Adapco[8], a leading industry in the field of developing CFD software provide the basic phenomenon of CFD analysis.

The engineering background of this study is the fluid flow study and the aerodynamic study in the field of aerospace and defence.

CHAPTER 3

COMPUTATIONAL FLUID DYNAMICS

3.1 The Strategy of CFD:

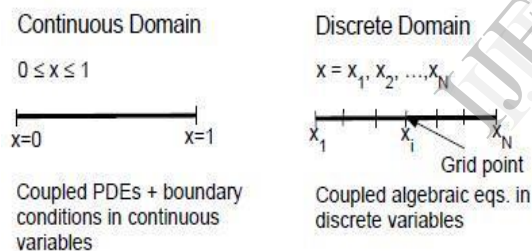
Broadly, the strategy of CFD is to replace the continuous problem domain with a discretized domain using a grid. In the continuous domain, each flow variable is defined

at every point in the domain. For instance, the pressure (p) in the continuous 1D domain shown in the Fig below would be given as

$$p = p(x), 0 < x < 1$$

In the discrete domain, each flow variable is defined only at the grid points. So, in the discretized domain shown below, the pressure would be defined only at the N grid points.

$$p_i = p(x_i), i = 1, 2, \dots, N$$



In a CFD solution, one would directly solve for the relevant flow variables only at the grid points. The values at other locations are determined by interpolating the values at the grid points.

The governing partial differential equations and boundary conditions are defined in terms of the continuous variables p, V etc. One can approximate these in the discrete domain in terms of the discrete variables p_i, V_i etc... The discrete system is a large set of coupled algebraic equations in the discrete variables. Setting up the discrete system and solving it (which is a matrix inversion problem) involves a very large number of repetitive calculations, a task we humans palm over to the digital computer.

3.2 Fluid characteristics:

Table 1: Fluid characteristics:

Macroscopic properties	Classification of fluid flows	
ρ Density μ viscosity p pressure T temperature V velocity	viscous compressible steady laminar single-phase	inviscid incompressible unsteady turbulent multiphase

The reliability of CFD simulations is greater

- For laminar/slow flow than for turbulent/fast ones
- For single-phase flows than for multi-phase flows
- For chemically inert systems than for reactive flows

3.3 CFD analysis process:

1. Problem statement --- information about the flow
2. Mathematical model --- IBVP = PDE + IC + BC
3. Mesh generation --- nodes/cells, time instants
4. Space discretization --- coupled ODE/DAE systems
5. Time discretization --- algebraic system $Ax=B$
6. Iterative solver --- discrete function values
7. CFD software --- implementation, debugging
8. Simulation run --- parameters, stopping criteria
9. Post processing --- visualization, analysis of data
10. Verification --- model validation / adjustment

3.3.1 Problem statement:

- What is known about the flow problem to be dealt with?
- What physical phenomena need to be taken into account?
- What is the geometry of the domain and operating conditions?
- Are there any internal obstacles or free surfaces/interfaces?
- What is the type of flow (laminar/turbulent, steady/unsteady)?
- What is the objective of the CFD analysis to be performed?
 - computation of integral quantities (lift, drag, yield)
 - Snapshot of field data for velocities, concentrations etc.
 - shape optimization aimed at an improved performance
- What is the easiest/cheapest/fastest way to achieve the goal?

3.3.2 Mathematical model:

1. Choose a suitable flow model (viewpoint) and reference frame.
2. Identify the forces which cause and influence the fluid motion.
3. Define the computational domain in which to solve the problem.
4. Formulate conservation laws for the mass, momentum, and energy.
5. Simplify the governing equations to reduce the computational effort:
 - use available information about the prevailing flow regime
 - check for symmetries and predominant flow directions (1D/2D)
 - neglect the terms which have little or no influence on the results
 - model the effect of small-scale fluctuations that cannot be captured
 - incorporate a priori knowledge (measurement data, CFD results)
6. Add constitutive relations and specify initial/boundary conditions.

3.3.3 Discretization Process

The PDE system is transformed into a set of algebraic equations

1. Mesh generation (decomposition into cells/elements)
 - Structured or unstructured, triangular or quadrilateral?
 - CAD tools + grid generators (Delaunay, advancing front)
 - mesh size, adaptive refinement in „interesting“ flow regions
2. Spaced discretization (approximation of spatial derivatives)
 - finite differences/volumes/elements
 - high-vs. low-order approximations
3. Time discretization (approximation of temporal derivatives)
 - explicit vs. implicit schemes, stability constraints
 - local time-stepping, adaptive time step control.

3.3.4 Iterative solution strategy:

The coupled nonlinear algebraic equations must be solved iteratively

- Outer iterations: the coefficients of the discrete problem are updated using the solution values from the previous iteration so as to
 - get rid of the nonlinearities by a Newton-like method
 - solve the governing equations in a segregated fashion
- Inner iterations: the resulting sequence of linear sub problems is typically solved by an iterative method

(conjugate gradients, multi grid) because direct solvers (Gaussian elimination) are prohibitively expensive.

- Convergence criteria: it is necessary to check the residuals, relative solution changes and other indicators to make sure that the iterations converge.

As a rule, the algebraic systems to be solved are very large (millions of unknowns) but sparse, i.e., most of the matrix coefficients are equal to zero.

3.3.5 CFD simulations:

The computing times for a flow simulation depend on

- The choice of numerical algorithms and data structures
- Linear algebra tools, stopping criteria for iterative solvers
- Discretization parameters (mesh quality, mesh size, time step)
- Cost per time step and convergence rates for outer iterations
- Programming language (most CFD codes are written in Fortran)
- Many other things (hardware, vectorization, parallelization etc.)

The quality of simulation results depends on

- The mathematical model and underlying assumptions
- Approximation type, stability of the numerical scheme
- Mesh, time step, error indicators, stopping criteria.

3.3.6 Post processing and analysis

Post processing of the simulation results is performed in order to extract the desired information from the computed flow field

- Calculation of derived quantities (stream function, vorticity)
- Calculation of integral parameters (lift, drag, total mass)
- Visualization (representation of numbers as images)
 - 1D data: function values connected by straight lines
 - 2D data: streamlines, contour levels, colour diagrams
 - 3D data: cut lines, cut planes, iso-surfaces, iso volumes
 - Arrow plots, particle tracing, animations.
- Systematic data analysis by means of statistical tools
- Debugging, verification, and validation of the CFD model.

3.4 Computational Meshes:

Degrees of freedom for the approximate solution are defined on a computational mesh which represents a subdivision of the domain into cells/elements

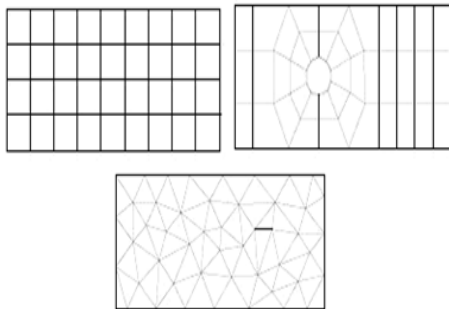


Fig 3.1: Computational Meshes.

3.4.1 Structured (regular) meshes:

- Families of gridlines do not cross and only intersect with other families once.
- Topologically equivalent to Cartesian grid so that each grid point (or CV) is uniquely defined by two indices in 2D or three indices in 3D, e.g., (i, j, k).
- Can be of type H (non periodic), O (periodic) or C (periodic with cusp)
- Limited to simple domains, local mesh refinement affects other regions.

3.4.2 Block-structured meshes:

- Multilevel subdivision of the domain with structured grids within blocks.
- Can be non-matching, special treatment is necessary at block interfaces.
- Provide greater flexibility, local refinement can be performed block wise.

3.4.3 Unstructured meshes

- Suitable for arbitrary domains and amenable to adaptive mesh refinement
- Consist of triangles or quadrilaterals in 2D, tetrahedra or hexahedra in 3D
- Complex data structures, irregular sparsity pattern, difficult to implement

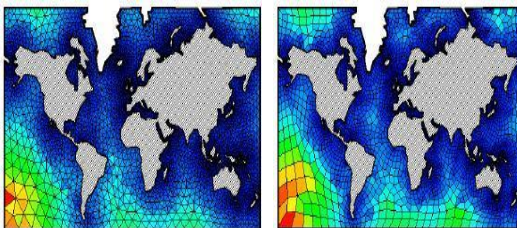
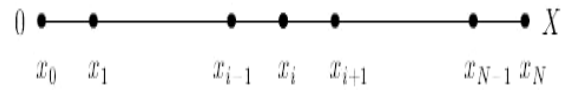


Fig 3.2: Structured and Unstructured Meshes

3.5 FINITE DIFFERENCE METHOD:

Principle: Derivatives in the partial differential equation are approximated by linear combinations of function values at the grid points.

1D: $\Omega = (0, X)$, $u_i \approx u(x_i)$
 $i = 0, 1, \dots, N$
 Grid points $x_i = i\Delta x$ mesh size $\Delta x = X/N$



3.6 Approximation of first-order derivatives:

Geometric interpretation

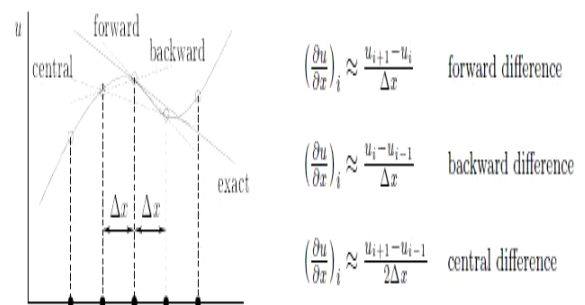


Fig3.7 Taylor series

3.7 Governing Equations of Fluid Dynamics:

It is important to understand the meaning and significance of each equation in order to develop a good numerical method and properly interpret the results. For the following physical principles the corresponding mathematical equations are used.

Mass is conserved -- Continuity equation

Newton's second law---Momentum equations

Energy is conserved--- Energy equations

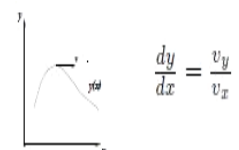
3.7.1 Description of fluid motion:

Eulerian: Monitor the flow characteristics in a fixed control volume.

Lagrangian: Track individual fluid particles as they move through the flow field.

Stream line: A streamline is a curve which is tangent to the velocity vector $v = (v_x, v_y, v_z)$ at every point. It is given by the relation

$$\frac{dx}{v_x} = \frac{dy}{v_y} = \frac{dz}{v_z}$$



Streamlines can be visualized by injecting tracer particles into the flow field

3.7.2 Summary of the governing equations:

1. Continuity equation / Law of conservation of mass

$$\frac{\partial \rho}{\partial t} + \nabla \cdot (\rho \mathbf{v}) = 0$$

2. Momentum equations / Newton's second law

$$\frac{\partial(\rho \mathbf{v})}{\partial t} + \nabla \cdot (\rho \mathbf{v} \otimes \mathbf{v}) = -\nabla p + \nabla \cdot \boldsymbol{\tau} + \rho \mathbf{g}$$

3. Energy equation / first law of thermodynamics

$$\frac{\partial(\rho E)}{\partial t} + \nabla \cdot (\rho E \mathbf{v}) = \nabla \cdot (\kappa \nabla T) + \rho q - \nabla \cdot (p \mathbf{v}) + \mathbf{v} \cdot (\nabla \cdot \boldsymbol{\tau}) + \nabla \mathbf{v} : \boldsymbol{\tau} + \rho \mathbf{g} \cdot \mathbf{v}$$

$$E = e + \frac{|\mathbf{v}|^2}{2}, \quad \frac{\partial(\rho e)}{\partial t} + \nabla \cdot (\rho e \mathbf{v}) = \nabla \cdot (\kappa \nabla T) + \rho q - p \nabla \cdot \mathbf{v} + \nabla \mathbf{v} : \boldsymbol{\tau}$$

This PDE system is referred to as the compressible Navier-Stokes equations

3.7.3 Generalized Form Of Governing Equation:

- $\partial/\partial t (\rho \Phi) + \nabla \cdot (\rho \vec{v} \Phi) = \nabla \cdot (\boldsymbol{\tau} \nabla \Phi) + S\Phi$
- $\partial/\partial t (\rho \Phi) =$ Transient form
- $\nabla \cdot (\rho \mathbf{v} \Phi) =$ Convection term
- $\nabla \cdot (\boldsymbol{\tau} \nabla \Phi) =$ Diffusion term
- $S\Phi =$ Source

Table 2: Generalized Form of Governing Equation

	Φ	$\boldsymbol{\tau}$	$S\Phi$
Continuity equation	1	0	0
Navier stokes equation in x-direction	u	μ	$-\delta P/\delta x + \rho f_x$
Navier stokes equation in y-direction	v	μ	$-\delta P/\delta y + \rho f_y$
Navier stokes equation in z-direction	w	μ	$-\delta P/\delta z + \rho f_z$
Energy equation	T	k/Cp	$S\Phi$

3.8 K-ε Model:

The K-epsilon model is one of the most common turbulence models, although it just doesn't perform well in cases of large adverse pressure gradients. It is a two equation model that means, it includes two extra transport equations to represent the turbulent properties of the flow. This allows a two equation model to account for history effects like convection and diffusion of turbulent energy.

The first transported variable is turbulent kinetic energy, the second transported variable in this case is the turbulent dissipation, it is the variable that determines the scale of the turbulence, whereas the first variable, determines the energy in the turbulence.

There are two major formulations of K-epsilon models. That of Launder and Sharma is typically called the "Standard" K-epsilon Model. The original impetus for the K-epsilon model was to improve the mixing-length model, as well as to find an alternative to algebraically prescribing turbulent length scales in moderate to high complexity flows.

The K-epsilon model has been shown to be useful for free-shear layer flows with relatively small pressure gradients. Similarly, for wall-bounded and internal flows, the model gives good results only in cases where mean pressure gradients are small; accuracy has been shown experimentally to be reduced for flows containing large adverse pressure gradients. One might infer then, that the K-epsilon model would be an inappropriate choice for problems such as inlets and compressors.

Usual K-epsilon models:

1. Standard k-epsilon model
2. Realisable k-epsilon model
3. RNG k-epsilon model

3.8.1 Standard k-epsilon model:

Transport equations for standard k-epsilon model:

For turbulent kinetic energy k

$$\frac{\partial}{\partial t}(\rho k) + \frac{\partial}{\partial x_i}(\rho k u_i) = \frac{\partial}{\partial x_j} \left[\left(\mu + \frac{\mu_t}{\sigma_k} \right) \frac{\partial k}{\partial x_j} \right] + P_k + P_b - \rho \epsilon - Y_M + S_k$$

For dissipation ε

$$\frac{\partial}{\partial t}(\rho \epsilon) + \frac{\partial}{\partial x_i}(\rho \epsilon u_i) = \frac{\partial}{\partial x_j} \left[\left(\mu + \frac{\mu_t}{\sigma_\epsilon} \right) \frac{\partial \epsilon}{\partial x_j} \right] + C_{1\epsilon} \frac{\epsilon}{k} (P_k + C_{3\epsilon} P_b) - C_{2\epsilon} \rho \frac{\epsilon^2}{k} + S_\epsilon$$

Modelling turbulent viscosity:

Turbulent viscosity is modelled as:

$$\mu_t = \rho C_\mu \frac{k^2}{\epsilon}$$

Production of k:

$$P_k = -\rho \overline{u_i' u_j'} \frac{\partial u_j}{\partial x_i}$$

$$P_k = \mu_t S^2$$

Where S is the modulus of the mean rate-of-strain tensor, defined as

$$S \equiv \sqrt{2 S_{ij} S_{ij}}$$

Effect of buoyancy:

$$P_b = \beta g_i \frac{\mu_t}{Pr_t} \frac{\partial T}{\partial x_i}$$

Where Prt is the turbulent Prandtl number for energy and gi is the component of the gravitational vector in the i'th direction. For the standard and realizable - models, the default value of Prt is 0.85.

The coefficient of thermal expansion, β, is defined as

$$\beta = -\frac{1}{\rho} \left(\frac{\partial \rho}{\partial T} \right)_p$$

Model constants:

$$C_{1e} = 1.44, C_{2e} = 1.92, C_{\mu} = 0.09, \sigma_k = 1.0, \sigma_{\epsilon} = 1.3.$$

CHAPTER 4

MODELLING, MESHING & SIMULATION OF THE OSPREY V22

For an aircraft the two main important parameters are the Lift Force and the Drag Force. For any aircraft or flying object,

- the Lift Force should be more than the Weight of the aircraft and
- The Drag Force should be less than the thrust on the aircraft.

This project deals with study of flow of compressible viscous flow over the VTOL osprey V22 aircraft and the Lift and Drag phenomenon of the aircraft is also studied. Also the variation of C_L & C_d with various angle of attack of the aircraft is studied using CFD methods.

4.1 Modelling of the V-22 Aircraft:

The modelling of the osprey V22 is done in SOLIDWORKS 2013. The whole assembly of the model consists of two parts –

1. Fuselage
2. Wing section.

The various sketch commands used are spline, ellipse, circle, etc., and some feature commands like extrude boss, extrude cut, revolve boss, revolve cut, loft, sweep, etc.

The Basic Dimensions of Osprey V22 are given below and shown diagrammatically in Fig 4.1

- Width, rotors turning, Ft. (m) -- 84.6 (25.78)
- Length, stowed, Ft. (m) -- 63.1 (19.23)
- Width, stowed, Ft. (m) -- 18.5 (5.64)
- Height, nacelles fully vertical, Ft. (m) -- 22.1 (6.74)
- Height, vertical stabilizer, Ft. (m) -- 17.65 (5.38)
- Length, fuselage, Ft. (m) -- 57.33 (17.48)

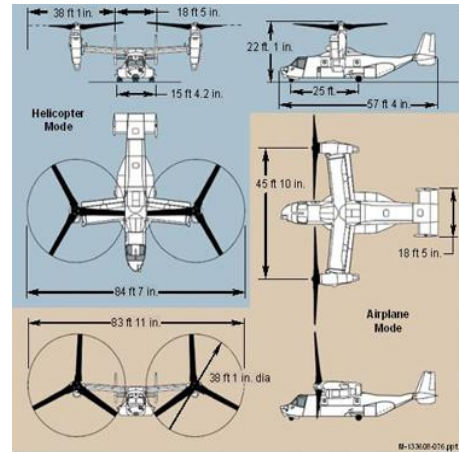


Fig4.1 Dimensions of Osprey V22

A solid model is created using the given dimensions to make a hollow shell for further analysis and scale ratio of 1:1450 is taken to model the final design.

4.1.1 Fuselage

The fuselage is an aircraft's main body section that holds crew, passengers and cargo. The following Fig 4.2 & 4.3 show the final model of V22 modelled in solidworks and part drawing of fuselage respectively.

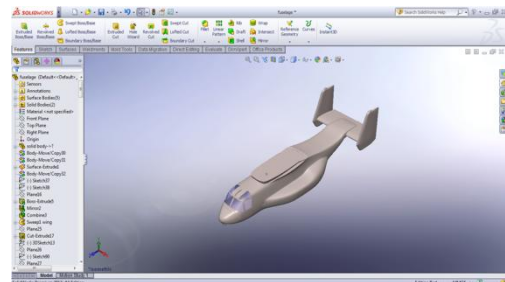


Fig4.2: Fuselage of Osprey V22

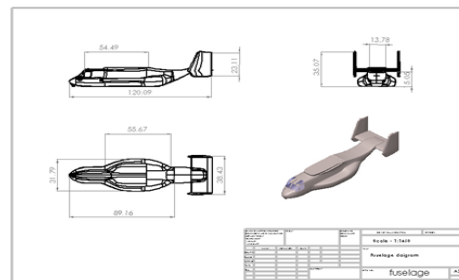


Fig4.3: Part drawings of fuselage

4.1.2 WINGS

A wing is a type of fin with a surface that produces aerodynamic force for flight or propulsion through the atmosphere, or through another gaseous or liquid fluid. As such, wings have an aerofoil shape, a streamlined cross-sectional shape producing a useful lift to drag ratio. For the osprey the engines are mounted at the ends of the

wings as seen in Fig4.4 &4.5, they are called as Nacelles. The Fig 4.4 &4.5 show the modelling and part drawing of wings respectively. Wings without the propellers are modelled for ease of CFD analysis. The rotors are not modelled to simulate the unpowered airframe aerodynamic wind tunnel testing.

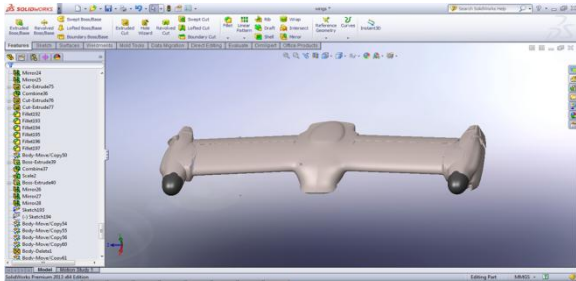


Fig4.4: Wings of osprey V22

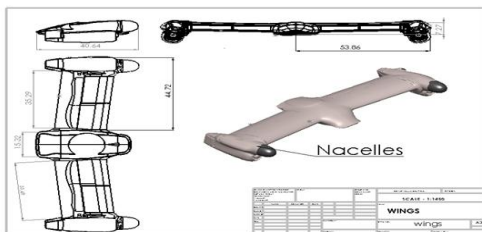


Fig4.5: Part drawing of wing

4.1.3 ASSEMBLY OF PARTS:

The two solid modelled parts (Fuselage & wings) are assembled using the assembly feature as shown in Fig 4.6, 4.7 &4.8. The interface between them is properly merged to avoid any form of discontinuities and extra projections which may alter the accuracy of the final result.

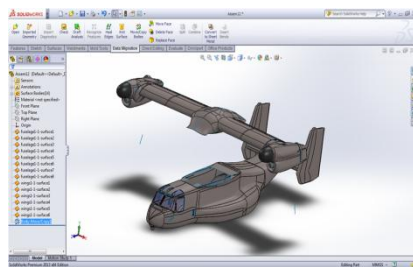


Fig4.6: Part assembly

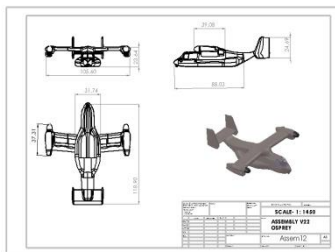


Fig4.7: Assembly Drawing

This completes the modelling of the aircraft and it looks as follows:



Fig4.8: Final model of Osprey V22

4.1.4 Modelling of the Continuum

The modelling of the continuum is done using ANSYS Workbench 14. The solid model is exported from SOLIDWORKS into ANSYS Workbench and then using the Enclosure option the block is created. The dimension of the enclosure is shown in Fig 4.9

Details View	
Details of Enclosure1	
Enclosure	Enclosure1
Shape	Box
Number of Planes	1
Symmetry Plane1	YZPlane
Model Type	Full Model
Cushion	Non-Uniform
<input type="checkbox"/> FD1, Cushion +X value (>0)	300 mm
<input type="checkbox"/> FD2, Cushion +Y value (>0)	350 mm
<input type="checkbox"/> FD3, Cushion +Z value (>0)	200 mm
<input type="checkbox"/> FD4, Cushion -X value (>0)	30 mm
<input type="checkbox"/> FD5, Cushion -Y value (>0)	150 mm
<input type="checkbox"/> FD6, Cushion -Z value (>0)	350 mm
Target Bodies	All Bodies
Merge Parts?	No

Fig4.9:Enclosure dimensions in Workbench

Once the enclosure is created using the Subtract Boolean operation the cavity of the aircraft is created in the block. Fig 4.10 shows the Boolean operation command and Fig 4.11 shows the final cavity created using the Boolean operation

Details View		
Details of Boolean1		
Boolean	Boolean1	
Operation	Subtract	
Target Bodies	1 Body	
Tool Bodies	Apply	Cancel
Preserve Tool Bodies?	No	

Fig4.10: Subtract using Boolean operation in Workbench.

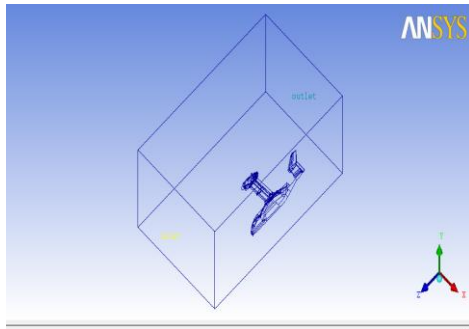


Fig4.11: Block with Aircraft in Workbench.

Once the block is created in ANSYS Workbench it is exported to ANSYS ICEM CFD 14, where in the meshing of the continuum is done.

4.2 Meshing and Simulation of the osprey v22

The generation of the Tetra/tri element mesh for Osprey V22.

- Extract feature curves from the symmetry plane.
- Create the material point.
- Generate the Octree mesh.
- Manipulate the mesh display using cut planes.
- Generate the Delaunay mesh.
- Smooth the mesh.
- Verify and save the mesh.

4.2.1 Meshing of the Continuum

The meshing of the continuum is done using ICEM CFD. The workbench file is first imported to ICEM CFD using the Workbench Reader option in the file menu as shown in Fig 4.12.

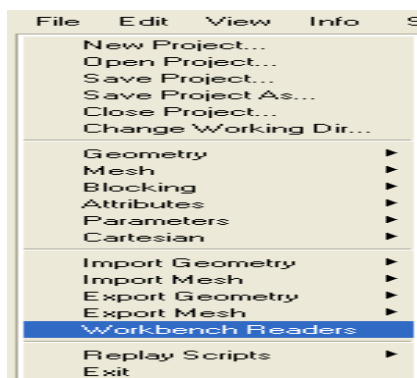


Fig 4.12: Workbench Reader option in ICEM CFD.

This opens a new window as shown in Fig 4.13 where in the location of the workbench file is to be given and then click ok. The model will be imported to ICEM CFD.

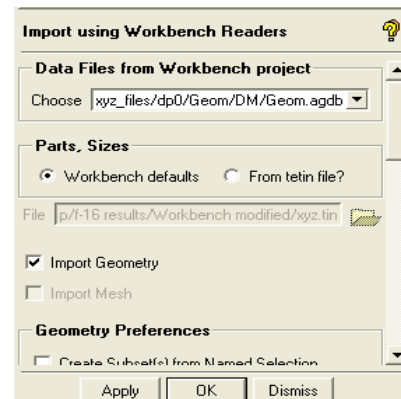


Fig 4.13: Workbench Import option in ICEM CFD.

Once the continuum is imported in ICEM CFD it looks as shown in Fig 4.14

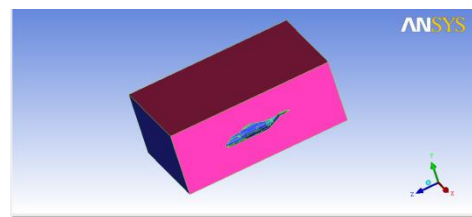


Fig 4.14: Imported Geometry in ICEMCFD

Now once the continuum is loaded then it should be divided into parts like osprey V22 for the fuselage, inlet, outlet and the rest as walls.

Then select mesh option as shown in Fig 4.15. Select the Global Mesh Setup icon in which the mesh size can be given.



Fig 4.15: Tool bar in ICEMCFD

Once the global mesh setup window as shown in Fig 4.16 opens give the element size as 4, size factor 1 and then click ok.

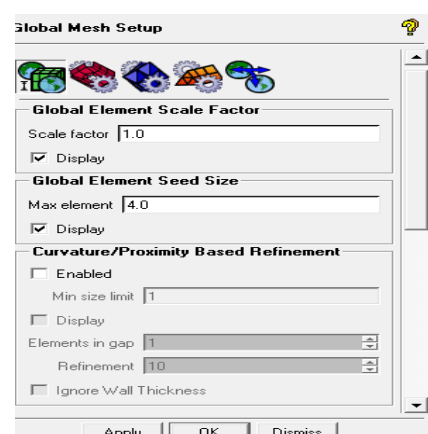


Fig 4.16: Global Mesh setup

Now the Part Mesh Setup Window as shown in Fig 4.17 opens and in this window for the fine mesh of the aircraft set the element size as 2 and then click on “apply” to apply changes.

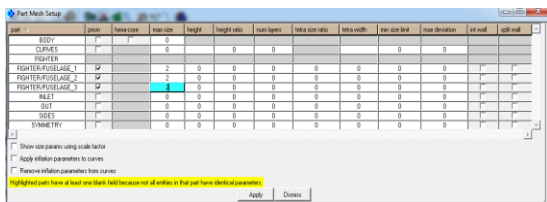


Fig4.17: Part Mesh setup

When all these parameters are set, click on the compute mesh icon to mesh the aircraft as shown in Fig 4.18



Fig4.18: Mesh tool bar

Now in the compute mesh window check if all the parameters are set to default and then click compute in volume mesh window. Once the meshing is done the continuum looks as shown in Fig 4.19.

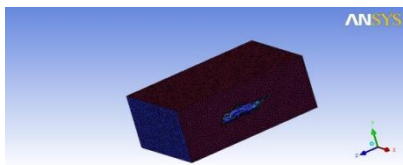


Fig 4.19: Meshed continuum

Once the meshing of the continuum is done this has to be exported to ANSYS Fluent 14, since Fluent is most widely used for flow analysis. To export it to Fluent the following steps are implemented.

First open the output window as shown in Fig 4.20.

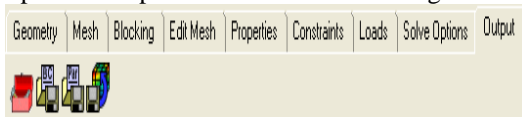


Fig4.20: Output tool bar

Open the solver setup window as shown in Fig 4.21

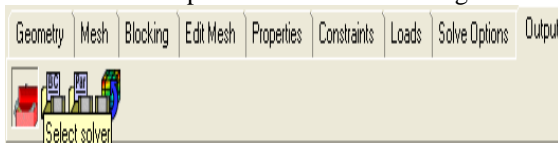


Fig4.21: solver setup tool bar

Then setup the solver settings. Select the output solver as Ansys Fluent and the common structural solver as Ansys as shown in Fig 4.22

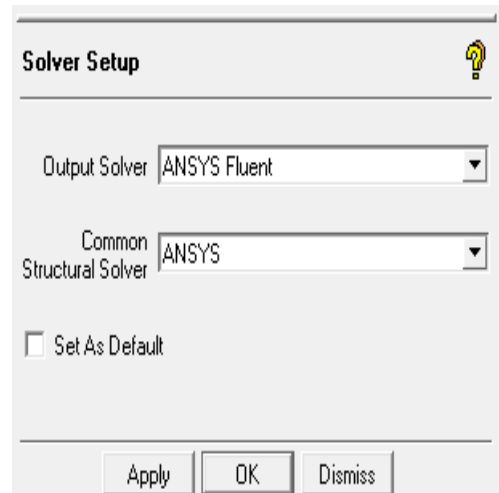


Fig4.22: Solver setup

Now assign the zones to the faces of the continuum as Inlet - Velocity inlet

Out - pressure outlet as shown in Fig 4.23

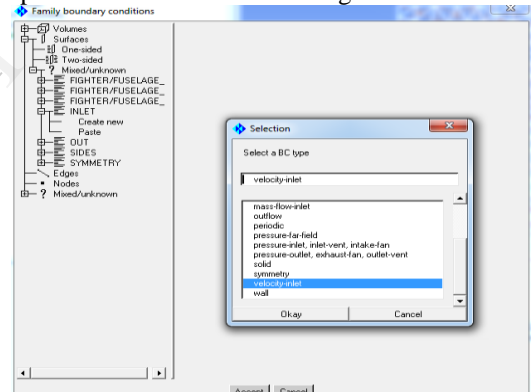


Fig4.23: Boundary conditions

Now this mesh file is to be written as input file for Fluent. For this the write input window is to be opened as shown in Fig 4.24. Enter the file name and then write it to Fluent as shown in Fig 4.24

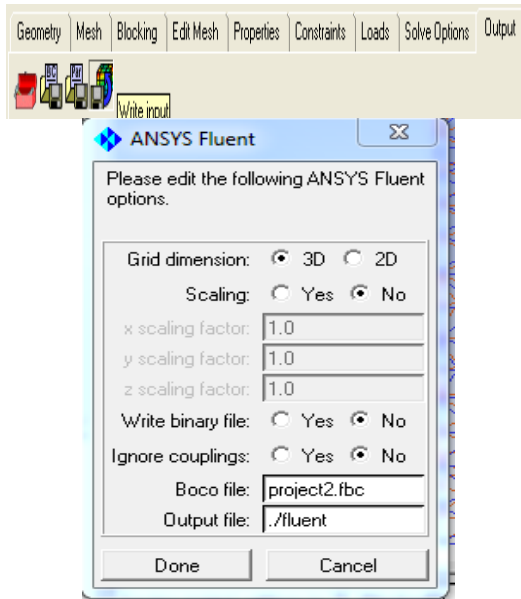


Fig4.24: Export to fluent

4.2.2 Simulation of the continuum

Simulation of this continuum is done in ANSYS Fluent 14. Once the model is exported to Fluent it is opened in Fluent and the required scaling is done and then the mesh is checked for any error and if no errors are found then the appropriate model for the simulation is assigned. The simulation is a **Density-based and steady state** simulation as shown in Fig 4.25

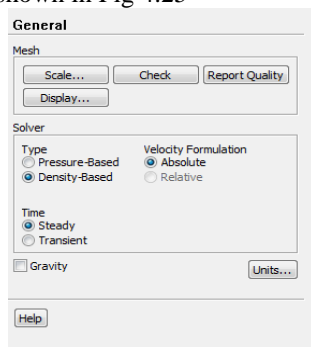


Fig4.25: Setting up the Model for the Simulation

The simulation model used is standard k-ε model as shown in Fig 4.26.

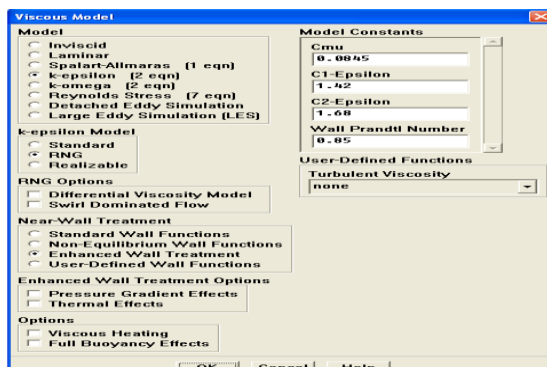


Fig4.26: Model setup

Material Properties

Once the model for the simulation is set then set the material properties for the flow field as Air. The material properties are set by default for the density of air as shown in Fig 4.27.

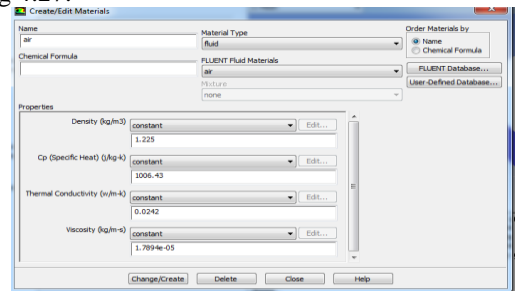


Fig4.27: Material Properties in ANSYS Fluent.

Boundary Conditions

After the material properties, the boundary conditions for the continuum is set as follows as shown in Fig 4.28

- For the inlet of the continuum, it is set as inlet-velocity and then click on edit. This opens a new window where in the velocity is set to 130ms⁻¹, normal to the boundary.

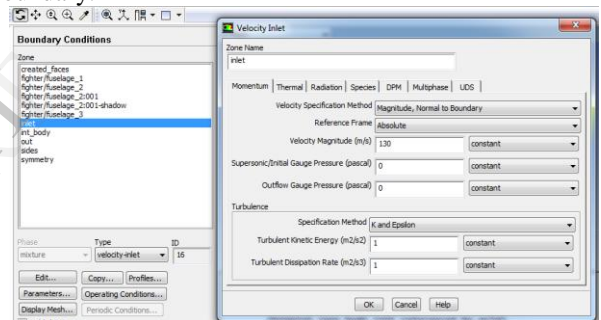


Fig4.28: Velocity-Inlet window in Fluent.

- For the outlet of the continuum, it is set to pressure-outlet and then click on edit. This opens a new window where in the values for the pressure are set to default as zero.
- Once these two are checked, set the sides of the continuum as standard walls.

Solution Stages

After assigning the material properties to the continuum, the solution stage of the simulation begins. In this solution stage, the solution methods, solution controls, monitors, solution initialization and running of the solution are done.

Solution Methods & Solution Controls

In solution methods the formulation is set to implicit Roe-FDS flux type and the turbulent kinetic energy, dissipation rate is set to first order upwind option and flow as second order upwind option as shown in Fig 4.29. In solution contours set the Courant Number is set to 5 & Set the modified turbulent viscosity to 0.8 as shown in Fig 4.30

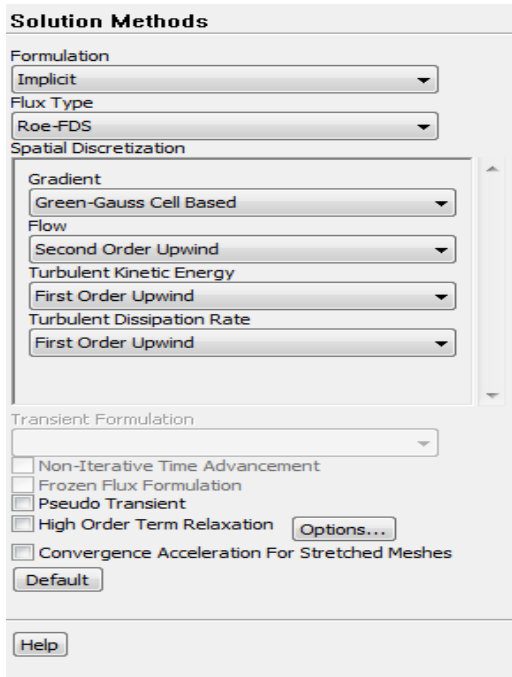


Fig 4.29: Solution Methods window

Solution Initialization

In solution initialization as shown in Fig 5.32, there are two initialization methods which are Hybrid Initialization and Standard Initialization. Since Standard Initialization requires longer computational time set solution initialization to Hybrid Initialization and the click on initialize.

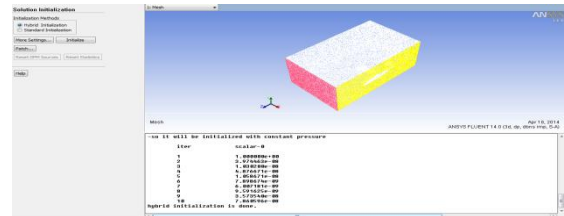


Fig4.32: Solution Initialization window in Fluent.

Run Calculation

In run calculation monitor set the number of iterations to 2000 and give the value for the auto save option as 50 and then click on calculate.

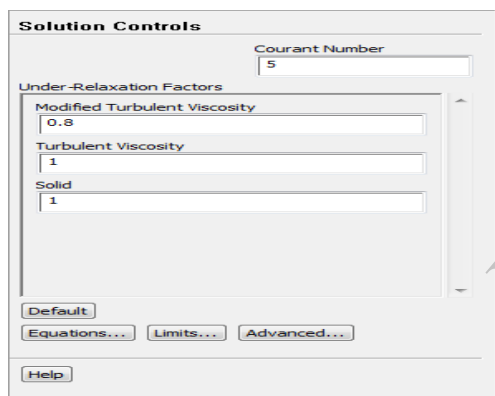


Fig4.30: Solution Control window

**CHAPTER 5
RESULTS AND DISCUSSIONS**

The fluid flow analysis over the V22 Osprey is conducted at different angle of attacks ranging from 0-18° and C_L C_d and Pressure distributions are observed. It is observed that solution converges at different iterations for different angle of attack of the model.

Table3: Full-scale flight conditions

Characteristic	Value
Mach	0.4
Angle of Attack	0°, 4°-16°
Nacelle	Airplane Mode
Flaps and Elevator	0°
Air Properties	Standard

Monitors

In the monitors panel create three monitor plots for Residuals, lift coefficient and drag coefficient. Then for each monitor set the required settings as shown in Fig4.31.

- For the lift & drag monitor click on edit and then select print to console, plot and write options. Also select fuselage1, fuselage 2, fuselage3 & out. Change the file name which is to be written to .txt format to get results in a text file

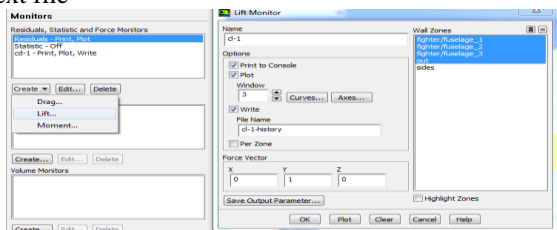


Fig4.31: Lift Coefficient window in Fluent.

The following figures show the Residual plot, C_L & C_d of Converged solution for angle of attack of 0°.

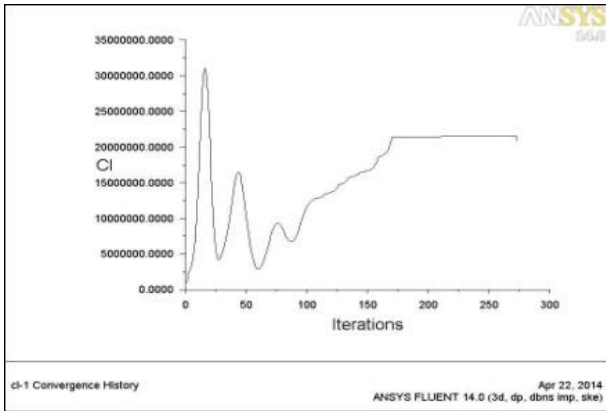


Fig 5.1: Convergence history of lift co-efficient at 0 angle of attack

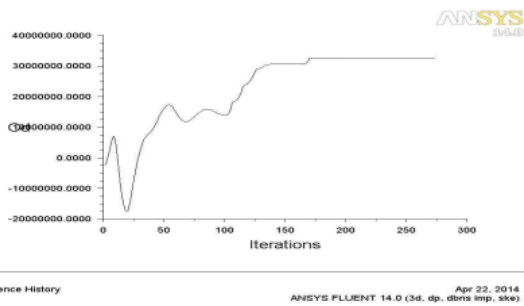


Fig 5.2: Convergence history of drag co-efficient at 0 angle of attack

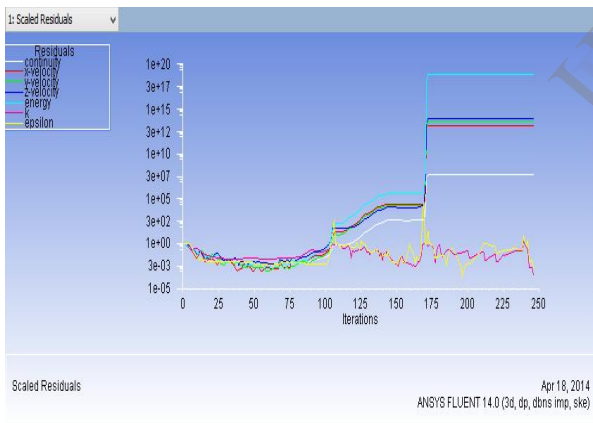


Fig5.3: Residuals convergence

The C_L & C_d values at different angles of attack, obtained from fluent are as follows

Table 4: C_L & C_d values at different angles of attack (with respect to the (0, 0) of the software used)

Angle of attack	C_L	C_d
0	2.15e+07	3.27e+07
4	1.09e+08	3.3612e+09
6	8.559e+08	1.77e+10
8	1.19e+06	1.29e+07
10	1.157E+06	1.866e+07
14	3.627e+06	1.143e+08
16	3.7292e+06	1.6524e+08
18	5.657e+09	2.153e+10
20	5.2535e+11	2.5137e+12

Coefficient of lift & Drag plots with variation in angles of attack:

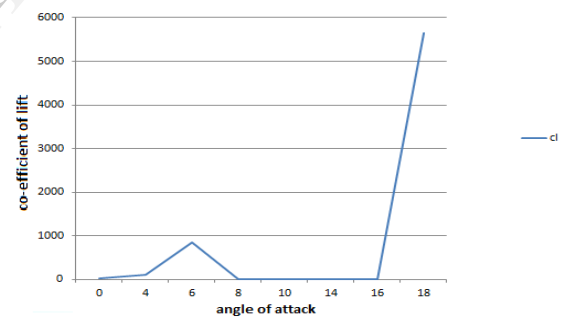


Fig 5.4: Variation of lift co-efficient (C_L) with increase in angle of attack

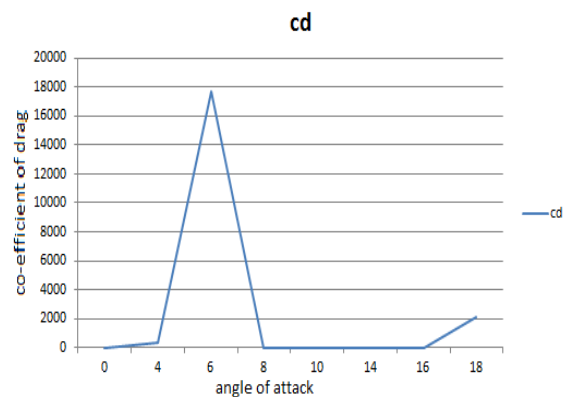


Fig 5.5: Variation of drag co-efficient (C_d) with increase in angle of attack

The aircraft lift coefficient, plotted in Fig 5.4 may be divided into three distinct regions predicted in the analyses. The low angle of attack data spans a range of 0° to 6° . In this region the lift increases with increase in angle of attack. the mid angle of attack region between 6° and 16° the lift value suddenly decrease and remains constant for certain period . Region between 4 and 8° shows a larger sensitivity to angle of attack changes. As before, angles of attack of greater than 16° exhibit more severe aircraft stall which must be avoided for optimal performance.

Similarly from Fig 5.6, the C_d values increase from $0-6^\circ$, fluctuate suddenly from $6-8^\circ$ and increases from the angles $8-16^\circ$. After 16° stall is observed where aircraft loses its cruising capability.

Pressure Plot:

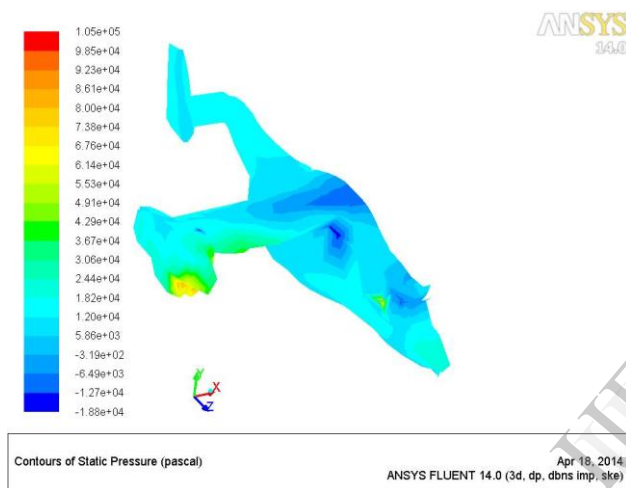


Fig5.6: Pressure plot

From Fig 6.6it is clear that at some places pressure is high as the aircraft design have sharp edges, corners and flat surfaces. This can be reduced by refining the design and seeing that there aren't any such errors in the geometry of the aircraft.

Streamlines from the fore-body strake for an angle of attack

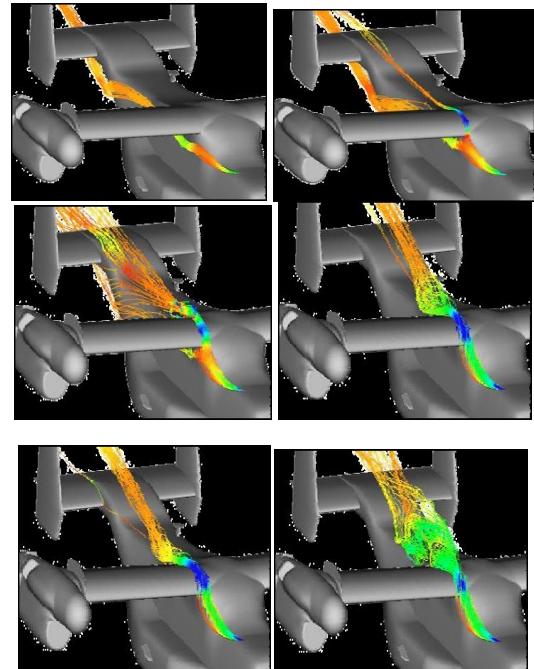


Fig5.7: Fluid flow on test object for different angle of attacks

TheFig 6.7 clearly depicts the reason why the C_L and C_d values abruptly change with respect to the angle of attack. At angles of attack less than 6° , the vortex from the strake passes below the wing; at 8° it begins to interact with the wing and by 10° the interaction is quite strong. From these streamline plots alone it is not completely clear what may be causing the increase in the horizontal tail liftan increase in effective angle of attack seen by the horizontal tail between 10° and 18° .ontribute to this phenomenon by deflecting the flow away from the tail, creating a lower pressure region above the tail. This lower pressure region then causes the higher pressure flow from below the wing to turn upward because of the local pressure gradient. This then turns the flow at the horizontal tail, increasing the local angle of attack and thus increasing the lift. This train of cause and effect is better supported by plots of the separated flow regions explicitly using oil line plots which depict surface flow patterns.

CHAPTER 6 CONCLUSIONS & FUTURE SCOPE

6.1 CONCLUSION

After conducting the Computational Fluid Dynamics Analysis for the osprey V22 Aircraft, this results are compared with the experimental results done by NASA and are mentioned in the paper “**Analysis of CFD Modelling Techniques over the MV-22 Tilt rotor** by Jennifer Abras, it is observed that

- C_L & C_d values increase with angle of attack up to 6° beyond which these coefficients change abruptly. From this we can see that the aircraft has best

performance in the angle of attacks ranging $0-8^{\circ}$ after which drag forces dominates , flow separation occurs which results in loss of lift and stall

- Variation between two results is due to Operating conditions which we considered are different are different from the one which is in the journal where the operation conditions are given as Mach no 0.3 & Altitude – 3000ft (operating pressure -90.8Kpa).
- One significant difference between the CFD geometry and the WT model is the presence of vortex generators (VGs) which span the entire wing including over the fuselage. The VGs are known to delay wing separation, but are difficult to model in CFD and have hence been omitted. The VGs are most likely the primary contributors to the differences in lift beyond 6° angle of attack.
- This difference is due in part to different predictions of the fore body/wing interaction between the two codes.
- The 23% thick wing provides additional challenges as separation occurs gently and relatively early as angle of attack is increased unless VGs are utilized.
- From the above streamline flow figures it has been observed that there is flow separation from angle 8° where the stall on the flight increases.

For many V-22 applications, RANS methods appear to be well suited to address difficult aerodynamic concerns. Ultimately however, careful evaluation of every solution is needed particularly for complex interactions and separated flows.

6.2 FUTURE SCOPE

The aerodynamic analysis of an aircraft is a vast field of research and development. Future work on this project will attempt aerodynamic study of this aircraft at different angles of rotation of nacelles. Further analysis can be done by adapting different aerofoils, studying unsteady effects at high angles of attack and the effect of turbulence models on these unsteady effects. The culmination of this work will be the analysis of the impact of the various aerodynamic components on the stability and control of the aircraft

REFERENCES

- [1] "Analysis of CFD Modelling Techniques over the MV-22 Tilt rotor" - Robert Nadrucci & Jennifer Abras ,pg. no. 15-150
- [2] Computational Fluid dynamics by John.D.Anderson , Second edition 2012 pg. 10-105
- [3] Aircraft design – A conceptual approach By Daniel.P.Raymer , 2nd edition 1992
- [4] Aerodynamics,Aeronautics, and Flight Mechanics by Barnes W. McCormick, Ph.D. , 2nd edition 1996 ,pg. no.125- 300
- [5] "A CFD Analysis of the Download Reduction for the V-22 osprey wing." – Chris Barnes
- [6] Help Tutorial Guide of ANSYS Fluent 14.
- [7] Boeing Image Gallery, "boeing.com/rotorcraft/military/v22/v22photos.html,"
- [8] Osprey Cad Model , "grabcad.com"